Information Horizons: AMERICAN Journal of Library And Information Science Innovation
Volume 4, Issue 08, 2026 ISSN (E): 2993-2777

Synthesis and Characterization, Cyclic Voltammetry Study, the Novel Thiadiazole Ligand Cobalt(II), Nickel(II), and Copper(II) Compounds, and In Vitro Anticancer Examination of the Ligand

Noor Lateef Kadim*
Department of Chemistry, College of Science, University of Thi-Qar, Nasiriyah, Thi-Qar 64001, Iraq
noor.lateef@utq.edu.iq

Zainab Majed Kareem
Department of Chemistry, College of Science, University of Thi-Qar, Nasiriyah, Thi-Qar 64001, Iraq
zainabmajeed454@utq.edu.iq

Abstract. *The thiadiazole (L2)-based ligand was readily synthesized with cobalt(II), nickel(II), and copper(II) and characterized using chemical and physical methods, supported by various spectroscopic techniques. Fourier transform infrared (FT-IR) and ultraviolet-visible spectroscopy, along with molar conductivity studies, confirmed the coordination pattern of the ligand with the metal ions, validating the proposed geometry of the complexes. Cyclic voltammetry studies were also conducted to understand the redox properties of the synthesized complexes. Redox pairs were identified, and the reversibility of the reaction was evaluated by calculating various electrochemical parameters, such as peak potential difference (ΔEp) and the ratio of anodic peak current to cathodic peak current (Ipa/Ipc). The results showed that the metal complexes exhibited promising redox properties, indicating the influence of the metal on the electron properties of the bond. A preliminary screening of the free linker was conducted on the HBL100 and MCF-7 breast cancer cell lines to investigate the role of co-localization in linker activity. Inhibition ratios were studied at specific concentrations rather than determining IC_{50} values. The resulting studies indicate that the synthesized thiadiazole metal complexes exhibit distinctive spectral properties attributable to a well-defined structure. The presence of biological activity, along with specific redox properties, makes them promising candidates for structural modification and intensive pharmacological studies to develop metalloprotein drug candidates for breast cancer treatment.*

Keywords: *1,3,4- thiadiazole, Metal Complexes, Spectroscopic Characterization, Cyclic Voltammetry (CV), Electron Density Distribution, Molar Conductivity, Anticancer Activity.*

Introduction

Heterocyclic compounds are of great importance in medicine and pharmaceutical chemistry due to their structural diversity and wide range of biological activities, which are crucial for research and treatment[1][2]. Among the most important of these compounds is the thiadiazole ring, particularly the 1,3,4-thiadiazole isomer, which is one of the most important sulfur-containing five-ring systems in drug design[3]. The great interest in the 1,3,4-thiadiazole ring stems from its biosimilarity to the pyrimidine ring, which forms the structural basis of the three nitrogenous bases that make up DNA[4][5]. This gives derivatives of this ring the ability to interfere with DNA replication. Furthermore, the mesoionic behavior of this ring allows it to penetrate biological membranes and

interact with target proteins efficiently. Numerous studies have shown that thiadiazole derivatives constitute an important class of heterocyclic compounds due to their wide range of biological activities, including antibacterial, antifungal, anti-inflammatory, antiviral, anticancer, anticonvulsant, and antioxidant properties. Antiviral activity, along with anticancer activity, is a highly significant area of research in this context, given the increasing global burden of cancer, as reported by the World Health Organization[6]. However, the interaction of organic bonds containing donor atoms such as sulfur and nitrogen, as in thiadiazole derivatives, with transition metal ions such as cobalt, nickel, and copper often leads to the formation of coordination complexes with distinct physical, chemical, and biological properties compared with free bonds[7][8]. This is exemplified by the chelation theory, which states that the metal's attachment to the bond increases the compound's ability to cross cell membranes and interact efficiently with a variety of biological targets, thus enhancing its biological activity compared to the unbonded bond. However, cyclic voltammetry is a useful analytical technique for studying the electrochemical behavior of these complexes, elucidating oxidation-reduction processes and electron transport mechanisms in the metal nucleus. This method provides precise information on the stability of different oxidation states of the metal and the reversibility of the electrochemical process. This enhanced biological performance is believed to be strongly linked to the mechanism of action of some metal complexes as anticancer agents in vivo. The enhanced physicochemical properties resulting from metal coordination may facilitate interactions with intracellular molecular targets, contributing to their therapeutic efficacy against cancer cells[9].

Thiadiazole compounds have been used as chelating agents to prepare metal complexes with multiple pharmaceutical and industrial applications. The sulfonamide derivatives associated with them have wide-ranging pharmaceutical applications as antimicrobials, anticancer agents, anti-obesity agents, and antithyroid agents, in addition to inhibiting enzymes and resisting inflammation and viruses[10]. A recent study published in 2025 in the journal ChemistrySelect showed that cobalt(II) complexes prepared from a Schiff base derived from 5-bromosalicylic aldehyde and 5-amino-1,3,4-thiadiazol-2-thiol exhibited the highest antifungal activity against Fusarium oxysporum and Candida albicans compared to nickel, cadmium, and zirconium complexes[11]. This class of compounds was also found to exhibit studyable electrical conductivity properties when doped with iodine. In a relatively recent study on bidental Schiff bases, a new ligand was prepared from the condensation of 2-amino-5-ethyl-1,3,4-thiadiazol with 4-(diethylamino)salicylaldehyde, and was used to prepare complexes of Pd(II), VO2+, Cu(II), and Ni(II)[12], and the spectroscopic and analytical results confirmed the proposed geometric formulas of these complexes. Copper complexes are the most common in the literature of this field due to the ease with which stable coordination bonds can be formed with the sulfur and nitrogen atoms in the ring. A recent study published in IJMS showed that the coordination-sensitive vibrational band in 1,3,4-thiadiazole rings is located in the 1450-1700 cm^{-1} region, and its positions and numbers differ significantly between the free ligand and its complex with copper, confirming the coordination of the heterocyclic ring nitrogen atoms with the copper(II) ion[13]. Another important study is related to the connection between the copper reaction and the formation of the thiadiazole ring itself. It was noted in a recent study (2024) that the copper-mediated reaction of thiadiazole derivatives derived from syringaldehyde led unexpectedly to the formation of a new thiadiazole ring during the complexation reaction with copper[14]. Density function theory (DFT) calculations supported this result by showing higher structural stability and lower reactivity of the resulting thiadiazole derivatives compared to the original thiadiazole derivatives. In a previous parallel study, Schiff bases of 2-amino-1,3,4-thiadiazole were prepared with various salicylaldehydes, followed by complexes of cobalt(II), copper(II), nickel(II), and zinc(II) at a molar ratio of 1:2. All of these complexes exhibited stability in air and limited solubility in organic solvents, except DMSO and DMF, exhibiting low molar conductivity values indicating their non-electrolyte nature[15][16]. A relatively old study (Part 91 of the Thiadiazole Studies Series) addressed the historical pharmacological significance of this ring, noting that 5-amino-1,3,4-thiadiazole-2-sulfonamide derivatives were historically used as diuretics, antiglaucoma, antiepileptic and ulcer drugs, and their metal complexes were used as inhibitors of zinc-containing carbonic anhydrase, while some copper(II) and zinc(II) complexes showed good antiepileptic activity in animal studies[17].

In light of the findings obtained, despite the fact that many thiadiazole derivatives and their compounds with transition metals have been studied due to their structural diversity and important biological properties, some crucial points have not been adequately addressed. In fact, most studies have been limited to the synthesis and spectroscopic investigations of these compounds. However, insufficient attention has been paid to integrating structural characterization with electrochemical investigations and assessing biological activity within a single integrated study[18][19]. In particular, the relationship between the electrochemical performance of metal thiadiazole compounds and their biological activity remains insufficiently understood. The electrochemical properties of these compounds influence their stability, electron transport capacity, and interactions with biological targets. Therefore, establishing relationships between cyclic voltammetry parameters and anticancer activity may contribute to understanding their potential mechanisms of action. However, previous studies have only rarely addressed these relationships. Furthermore, comparative studies examining cobalt(II), nickel(II), and copper(II)-based thiadiazole compounds linked by the same thiadiazole bond under identical experimental conditions are rare. Consequently, the role of the associated metal ion in determining the structural, electrochemical, and biological properties of these compounds has not yet been fully elucidated. While several thiadiazole derivatives have been evaluated for their activity against various cancer cell lines, no research has been published on their activity against the HBL100 breast cancer cell line. This highlights the need for further research to assess the biological potential of these compounds and to investigate the possible relationship between their molecular structure, redox properties, and antiproliferative activity. Therefore, this work aims to fill this gap by synthesizing novel cobalt(II), nickel(II), and copper(II)-based thiadiazole compounds and then examining their spectral properties and electrochemical behavior using cyclic voltammetry. Additionally, a preliminary biological evaluation was performed on the MCF-7 HBL100 breast cell line. Overall, this integrated approach should provide a broader understanding of how coordination chemistry, redox properties, and biological function are interconnected and influence one another.

Methodology

Preparation of 5-Hydrazinyl-1,3,4-thiadiazol-2-amine

Step 1: Preparation of Dipotassium 1,3,4-thiadiazole-2,5-bis(thiolate)

As shown in **Scheme 1,** potassium hydroxide (11.2 g, 0.2 mol) was dissolved in ethanol (100 mL) and transferred to a 150 mL spherical-bottom flask. Hydrazine hydrate (5 mL, 0.1 mol) was then added, and the reaction mixture was heated until completely dissolved. The mixture was then cooled in an ice bath to approximately 2 °C. Carbon disulfide (15.2 mL, 0.2 mol) was added in batches, and the reaction mixture was heated under reflux for 20 hours. The progress and completion of the reaction were monitored by the cessation of hydrogen sulfide gas release, using lead acetate solution as an indicator. Once the reaction was complete, the crude ethanol was recrystallized to obtain pale yellow, needle-like crystals of dipotassium 1,3,4-thiadiazol-2,5-di(thiols) [20]. The product showed a melting point between 260 and 262 degrees Celsius and was obtained at 89%.

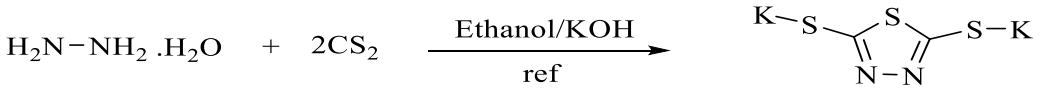

potassium 1,3,4-thiadiazole-2,5-bis(thiolate)

Step 2: Preparation of 1,3,4-thiadiazole-2,5-dithiol

The substance was taken after the solution had been evaporated by half. A quantity of cold water was then added to dissolve the formed salt, followed by acidifying the resulting solution using 10% hydrochloric acid until a light yellow precipitate was formed. The precipitate was filtered, washed with cold water, and recrystallized with ethanol to obtain compound C in the form of needle-like crystals with a melting point of 0°C (164-166°C) and a reaction yield of 75% [21]. As shown in **Scheme 2.**

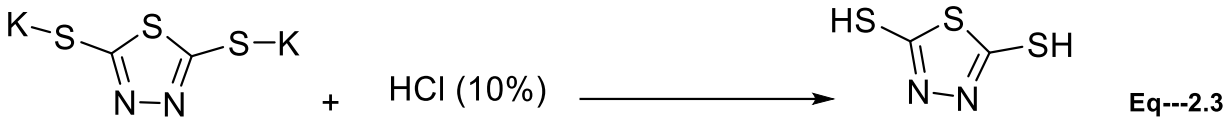

Eq---2.3

1,3,4-thiadiazole-2,5-dithiol

Step 3: Reaction with Hydrazine Hydrate ($NH_2NH_2.H_2O$)

As shown in **Scheme 3** and **Table 1**, the compound (10 g, 0.1 mol) was reacted with hydrazine hydrate (8 mL, 0.2 mol) in a 100 mL spherical-bottom flask using ethanol (50 mL) as the solvent. The reaction was carried out under reflux for 25 hours, and its progress was monitored by observing the release of hydrogen sulfide gas using filter paper saturated with lead acetate solution. After the reaction was complete, the resulting precipitate was collected by filtration, giving the compound as a yellowish-white solid. The product exhibited a melting point between 199 and 201 °C and was obtained in 83% [22] [23].

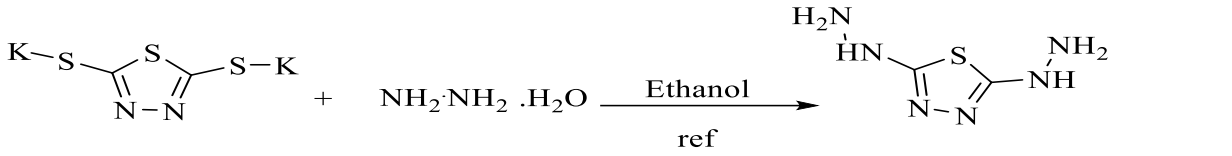

2,5-dihydrazineyl-1,3,4-thiadiazole

Table 1: Molecular Formula, Structural Formula, and Selected Physical Properties of the Synthesized Compounds

Compound	Formula	M. wt	Color	M. pc	Yield%	Rf
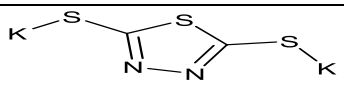	$C_2N_2S_3K_2$	226	Pale Yellow	260-262	89	0.69
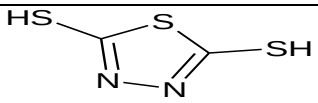	$C_2H_2N_2S_3$	150	Light Yellow	164-166	84	0.83
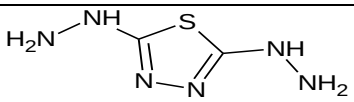	$C_2H_6N_6S$	146	Off-white	199-201	83	0.77

Preparation of Ligand L_2

The bond was prepared by reacting the compound (1.5 g, 0.0102 mol) with aldehyde (L2) at a molar ratio of 1:2. The compound was mixed with 2,4-dimethoxybenzaldehyde (2.3 ml) in a 100 mL reaction flask, and the reaction mixture was then dissolved in ethanol (60 mL) [24]. The reaction pathway was monitored by thin-layer chromatography (TLC) using a mixture of ethyl acetate and hexane as the solvent (3:7, Rf value). After the reaction was completed after 6 hours, the resulting mixture was cooled and filtered. The resulting precipitate was recrystallized from ethanol [25] to obtain yellow crystals. The synthesized compound exhibited a melting point between 188 and 190 °C and was obtained in 80% of cases, as shown in **Scheme 4**.

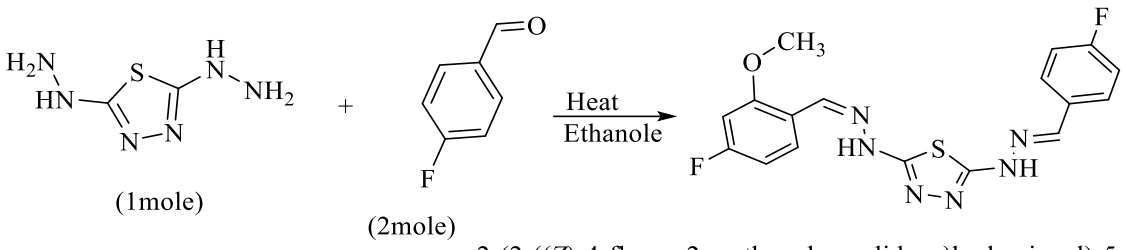

2-(2-((*Z*)-4-fluoro-2-methoxybenzylidene)hydrazineyl)-5-(2-((*E*)-4-fluorobenzylidene)hydrazineyl)-1,3,4-thiadiazole

Preparation of Metal Complexes

As described below, cobalt(II), nickel(II), and copper(II) complexes were prepared by the complex formation reaction of the corresponding metal ions with a 1:1 (metal) synthesized bond. In a 100 mL spherical-bottom flask, the (L_2) synthesized bond (1 mmol), dissolved in ethanol (50 mL), was mixed separately with 1 mmol of the corresponding transition metal salts. The complex formation reaction mixtures were heated under reflux with continuous stirring for 2–3 hours, and the progress of the reactions was monitored by thin-layer chromatography (TLC). After the complex formation reactions were complete, colored precipitates formed [26]. The precipitated complexes were filtered and washed with distilled water to remove any excess metal salts. The physical properties of the prepared compounds are shown in Table 2 below.

Table 2: Molecular Formulas and Selected Physical Properties of Ligand L_2 and Its Metal Complexes

NO.	Formula	M.wt	color	M.pc	Yield %
L_2	$C_{16}H_{12}N_6SF_2$	358	Yellow	188-190	80
1	$[Co(L_2)Cl_2.2H_2O]$	524	Light Brown	202-204	88.4
2	$[Ni(L_2)Cl_2.2H_2O]$	524	Pale Yellow	198-200	82.3
3	$[Cu(L_2)Cl_2.2H_2O]$	528	Light Yellow	207-210	65.2

Results and Discussion

1-FT-IR Spectra of Ligands L_2 and Metal Complexes

Characteristic Fourier transform infrared (FT-IR) spectral data are shown in Table 6 and Figures 1–4. The L2 ligand exhibited a broad band centered at 3145 cm^{-1}, which was attributed to N–H bond stretching [27]. Characteristic bands associated with CH=N and C=N bond stretching vibrations were also observed at 1600 and 1627 cm^{-1}, respectively. Additionally, the symmetric stretching vibration of the C–S–C group appeared at 1226 cm^{-1}. The spectra of the metal complexes showed marked shifts in the positions and intensity of the ligand bands, particularly those attributed to the C=N and CH=N groups, confirming their coordination with the metal ions [28]. Furthermore, new absorption bands attributable to M–O and M–N stretching vibrations appeared at approximately 615 and 511 cm^{-1}, respectively, while M–Cl stretching bands appeared within the 424–426 cm^{-1} region, consistent with the proposed coordination pattern.

Table 3: FT-IR Spectra of Ligand L_2 and Complexes

Group	L_2	CoL_2	NiL_2	CuL_2
N-H	**3145**	**3149**	**3115**	**3149**
C-H (aromatic)	**3061**	**3061**	**3059**	**3061**
C=N (Azo)	**1627**	**1629**	**1629**	**1629**

CH=N (endo)	**1600**	**1598**	**1598**	**1600**
C-SC (sy)	**1153**	**1153**	**1153**	**1153**
C-SC (asy)	**1226**	**1226**	**1226**	**1226**
Structural Movement	**1016**	**1012**	**1012**	**1012**
C-F	**1319**	**1321**	**1319**	**1319**
M-N	**---**	**511**	**511**	**511**
M-Cl	**---**	**426**	**426**	**424**
M-O	**---**	**615**	**615**	**615**

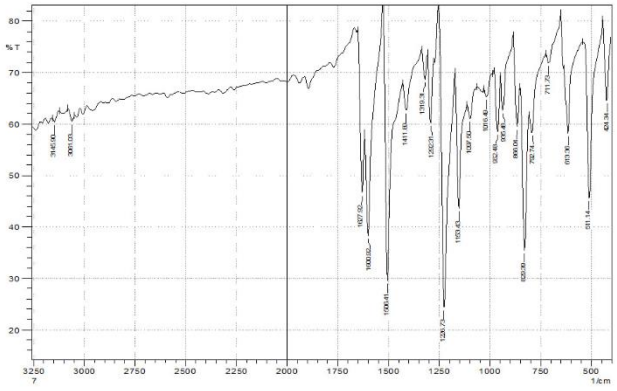

Figure 4: FT-IR spectrum of L_2

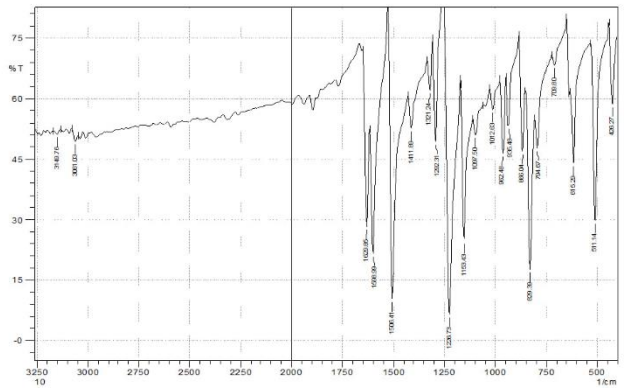

Figure 3: FT-IR spectrum of CoL_2

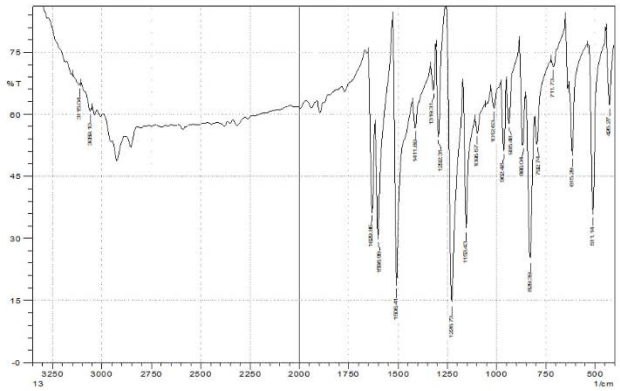

Figure 2: FT-IR spectrum of NiL_2

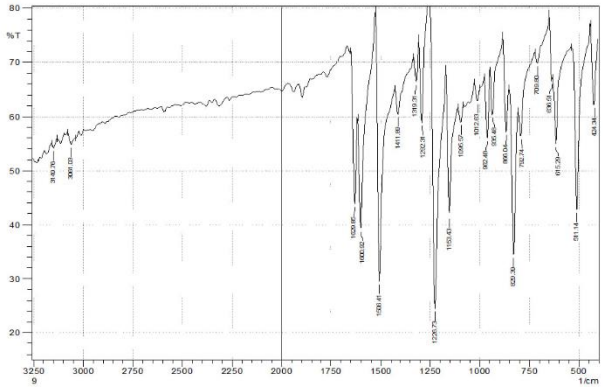

Figure 1: FT-IR spectrum of CuL_2

2-^{1}H and ^{13}C NMR Spectra of Ligand L_2

In the proton nuclear magnetic resonance (^{1}H NMR) spectrum, as shown in **Table 7** and **Figure 5**, a broad resonance at δ 9.99 ppm was attributed to the NH proton, its breadth being due to proton exchange [29]. The azomethine (CH=N) proton appeared as a characteristic signal at δ 8.72 ppm, consistent with the removal of the protective shield of the neighboring nitrogen atom and the conjugated electron system. Signals in the δ 7.95–7.94 ppm range are attributed to the protons of the two carbon atoms near the fluorine-containing carbon atom in the aromatic ring. Signals in the δ 7.36–7.35 ppm range are attributed to the protons of the two carbon atoms far from the fluorine-containing carbon atom in the aromatic ring, which are tetravalent.

As shown in **Table 7** and **Figure 6**, the proposed chemical structure was also confirmed by ^{13}C-NMR spectroscopy. A characteristic resonance of the azomethine carbon (C=N) was observed at δ 161.07 ppm [30] [31]. The signal at the higher end of the aromatic region, especially δ 136.50 and 133.09 ppm, corresponds to aromatic carbons influenced by the fluorine atom, while the signals at δ 130.50 and 129.57 ppm are for other aromatic carbons within the ring.

Table 4: ^{1}H and ^{13}C NMR Spectra of Ligand L_1

Structural formulas	**Type of NMR**	**NMR Data of (L_1)**
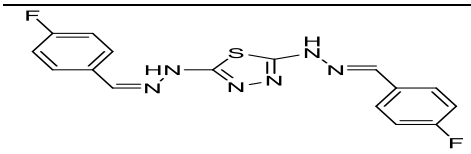	^{1}H-NMR	δ 9.99 (2H, br s, NH), 8.72 (2H, s, CH=N), 7.95,7.94 (4H, m, Ar-H), 7.74–7.35 (4H, m, Ar-H) ppm
	^{13}C-NMR	δ 161.07 (C=N), 136.50, 133.09 (Ar-C influenced by F), 130.50, 129.57 (Ar-C) ppm

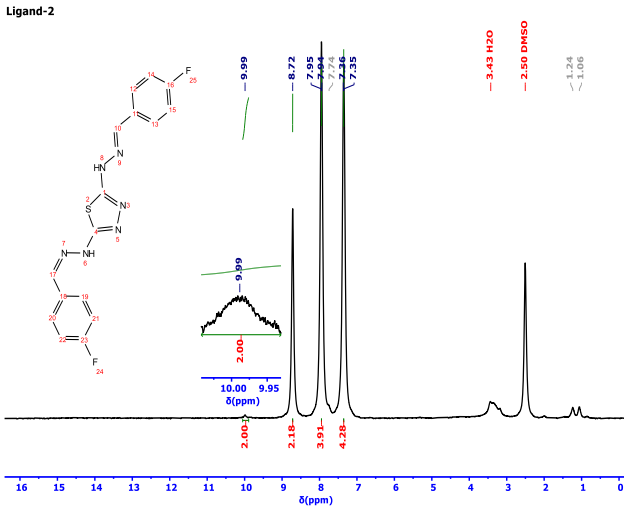

Figure 5: ^{1}H-NMR of L_2

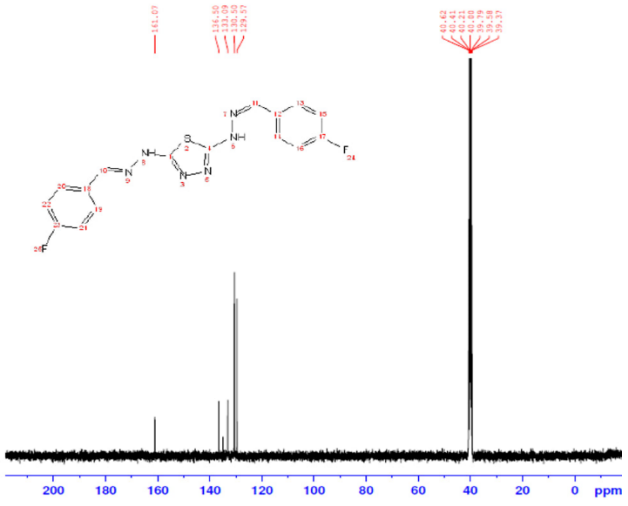

Figure 6: ^{13}C-NMR of L_2

3-Mass Spectra

The full mass spectrometry (L2) data and proposed dissociation pathways for the synthesized compounds are shown in **Figures 7–10** and **Tables 8–11**. Their metal complexes provided further evidence for the proposed molecular structures. Molecular ion (M^+) peaks were observed at m/z 358 for the L2 linker, m/z 524 for the cobalt(II) and nickel(II) complexes, and m/z 528 for the copper(II) complex, in good agreement with their calculated molecular weights [32]. A base peak was detected at m/z 149, corresponding to the dissociation ion $[C_8H_9N_2O]^{\bullet}$, except for the cobalt complex at the peak of m/z 245, and its dissociation ion $[C_0H_{10}N_{16}S_{16}]^{\bullet}$ [33].

Table 5: Mass fission of L_2 ligand

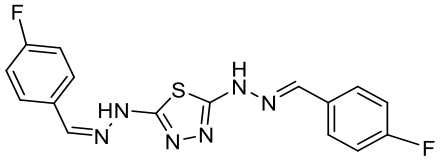 Chemical Formula: $C_{16}H_{12}F_2N_6S$ Exact Mass: 358.1 Molecular Weight: 358.4	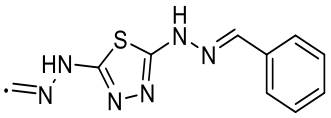 Chemical Formula: $C_{10}H_8FN_6S^{\bullet}$ Exact Mass: 263.1 Molecular Weight: 263.3	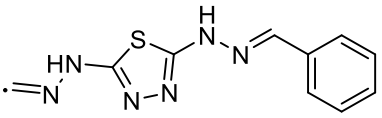 Chemical Formula: $C_{10}H_9N_6S^{\bullet}$ Exact Mass: 245.1 Molecular Weight: 245.3
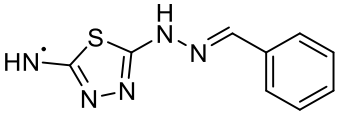 Chemical Formula: $C_9H_8N_5S^{\bullet}$ Exact Mass: 218.1 Molecular Weight: 218.3	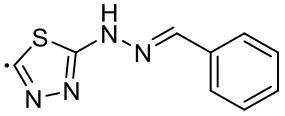 Chemical Formula: $C_9H_7N_4S^{\bullet}$ Exact Mass: 203.0 Molecular Weight: 203.2	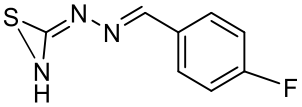 Chemical Formula: $C_8H_6FN_3S$ Exact Mass: 195.0 Molecular Weight: 195.2
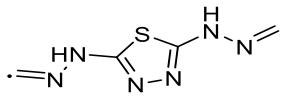 Chemical Formula: $C_4H_5N_6S^{\bullet}$ Exact Mass: 169.0 Molecular Weight: 169.2	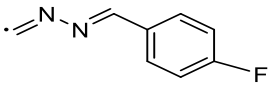 Chemical Formula: $C_8H_6FN_2^{\bullet}$ Exact Mass: 149.1 Molecular Weight: 149.1	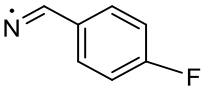 Chemical Formula: $C_7H_5FN^{\bullet}$ Exact Mass: 122.0 Molecular Weight: 122.1
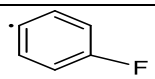 Chemical Formula: $C_6H_4F^{\bullet}$ Exact Mass: 95.0 Molecular Weight: 95.1		

Table 6: Mass fission of CoL_2

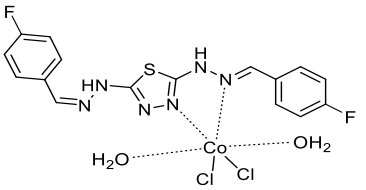 Chemical Formula: $C_{16}H_{16}Cl_2CoF_2N_6O_2S$ Exact Mass: 523.0 Molecular Weight: 524.2	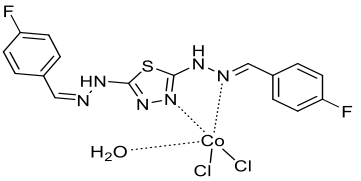 Chemical Formula: $C_{16}H_{14}Cl_2CoF_2N_6OS$ Exact Mass: 505.0 Molecular Weight: 506.2	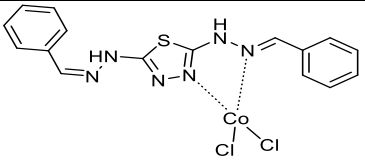 Chemical Formula: $C_{16}H_{14}Cl_2CoN_6S$ Exact Mass: 451.0 Molecular Weight: 452.2
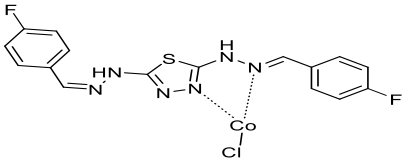 Chemical Formula: $C_{16}H_{12}ClCoF_2N_6S$ Exact Mass: 452.0 Molecular Weight: 452.8	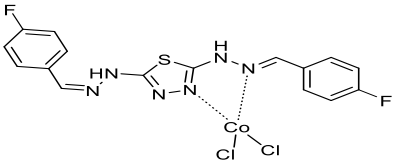 Chemical Formula: $C_{16}H_{12}Cl_2CoF_2N_6S$ Exact Mass: 487.0 Molecular Weight: 488.2	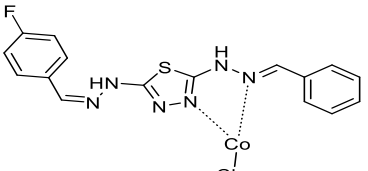 Chemical Formula: $C_{16}H_{13}ClCoFN_6S$ Exact Mass: 434.0 Molecular Weight: 434.8

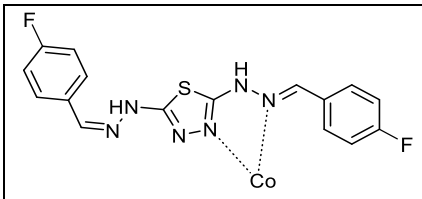 Chemical Formula: $C_{16}H_{12}CoF_2N_6S$ Exact Mass: 417.0 Molecular Weight: 417.3	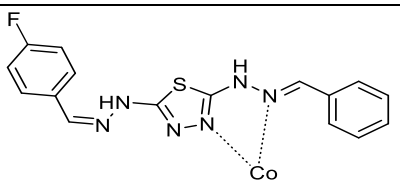 Chemical Formula: $C_{16}H_{13}CoFN_6S$ Exact Mass: 399.0 Molecular Weight: 399.3	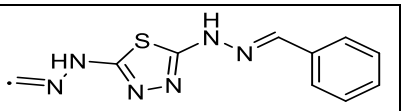 Chemical Formula: $C_{10}H_9N_6S^{\bullet}$ Exact Mass: 245.1 Molecular Weight: 245.3
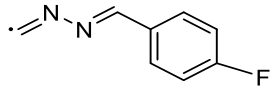 Chemical Formula: $C_8H_6FN_2^{\bullet}$ Exact Mass: 149.1 Molecular Weight: 149.1		

Table 7: Mass fission of NiL_2

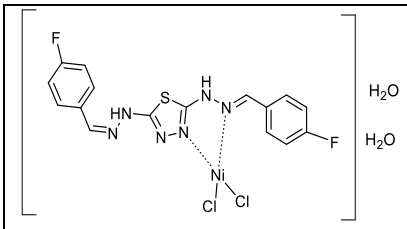 Chemical Formula: $C_{16}H_{16}Cl_2F_2N_6NiO_2S$ Exact Mass: 522 Molecular Weight: 524	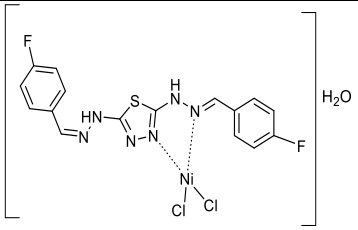 Chemical Formula: $C_{16}H_{14}Cl_2F_2N_6NiOS$ Exact Mass: 504 Molecular Weight: 506	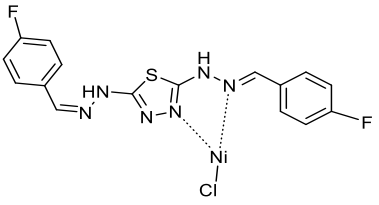 Chemical Formula: $C_{16}H_{12}ClF_2N_6NiS$ Exact Mass: 451.0 Molecular Weight: 452.5
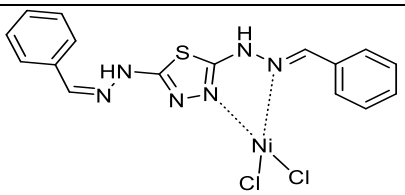 Chemical Formula: $C_{16}H_{14}Cl_2N_6NiS$ Exact Mass: 450.0 Molecular Weight: 452.0	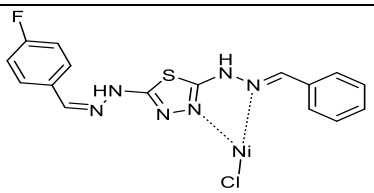 Chemical Formula: $C_{16}H_{13}ClFN_6NiS$ Exact Mass: 433.0 Molecular Weight: 434.5	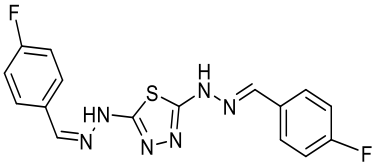 Chemical Formula: $C_{16}H_{12}F_2N_6S$ Exact Mass: 358.1 Molecular Weight: 358.4
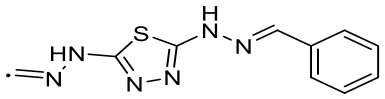 Chemical Formula: $C_{10}H_9N_6S^{\bullet}$ Exact Mass: 245.1 Molecular Weight: 245.3	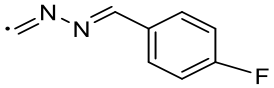 Chemical Formula: $C_8H_6FN_2^{\bullet}$ Exact Mass: 149.1 Molecular Weight: 149.1	

Table 8: Mass fission of CuL_2

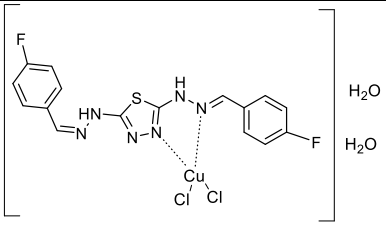 Chemical Formula: $C_{16}H_{16}Cl_2CuF_2N_6O_2S$ Exact Mass: 527 Molecular Weight: 529	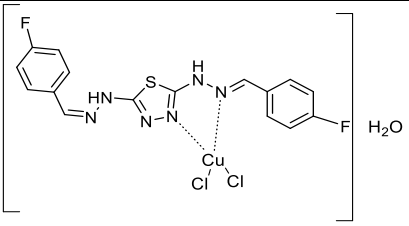 Chemical Formula: $C_{16}H_{14}Cl_2CuF_2N_6OS$ Exact Mass: 509 Molecular Weight: 511	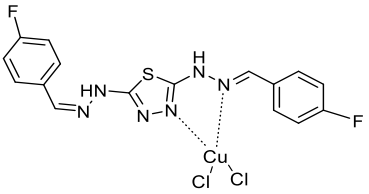 Chemical Formula: $C_{16}H_{12}Cl_2CuF_2N_6S$ Exact Mass: 490.9 Molecular Weight: 492.8
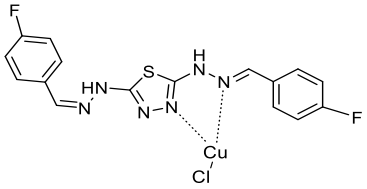 Chemical Formula: $C_{16}H_{12}ClCuF_2N_6S$ Exact Mass: 456.0 Molecular Weight: 457.4	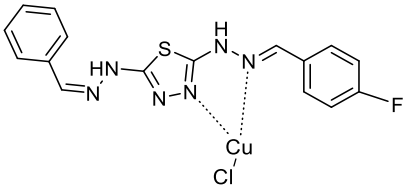 Chemical Formula: $C_{16}H_{13}ClCuFN_6S$ Exact Mass: 438.0 Molecular Weight: 439.4	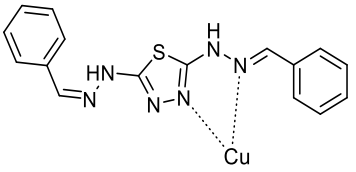 Chemical Formula: $C_{16}H_{14}CuN_6S$ Exact Mass: 385.0 Molecular Weight: 385.9
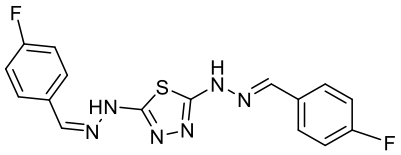 Chemical Formula: $C_{16}H_{12}F_2N_6S$ Exact Mass: 358.1 Molecular Weight: 358.4	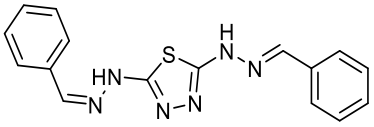 Chemical Formula: $C_{16}H_{14}N_6S$ Exact Mass: 322.1 Molecular Weight: 322.4	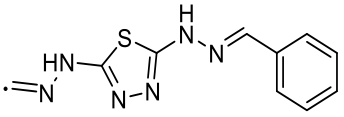 Chemical Formula: $C_{10}H_9N_6S^{\bullet}$ Exact Mass: 245.1 Molecular Weight: 245.3
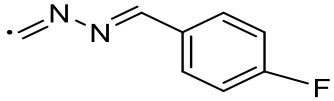 Chemical Formula: $C_8H_6FN_2^{\bullet}$ Exact Mass: 149.1 Molecular Weight: 149.1		

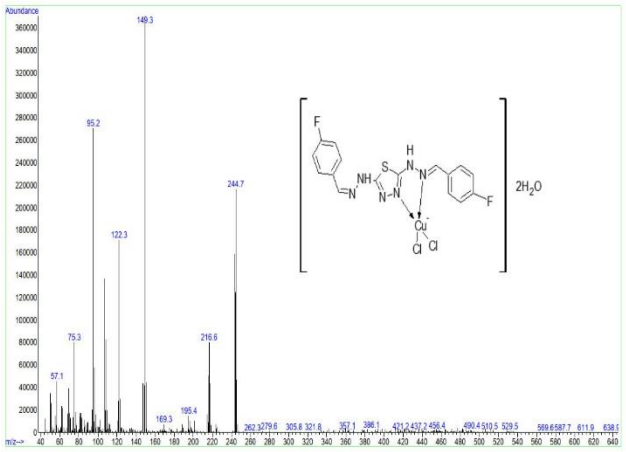

Figure 8: Mass spectrum of L_2

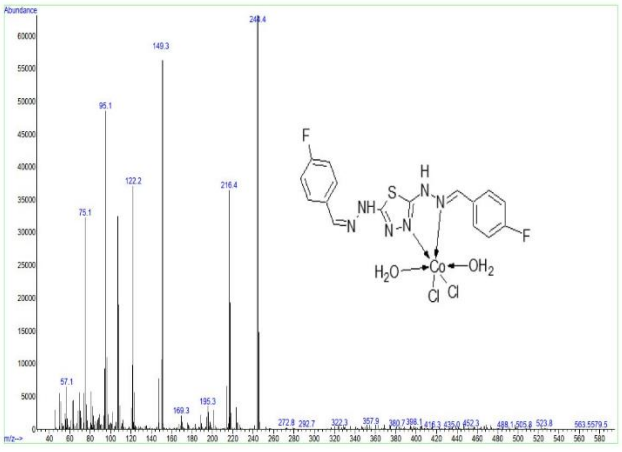

Figure 7: Mass spectrum of CoL_2

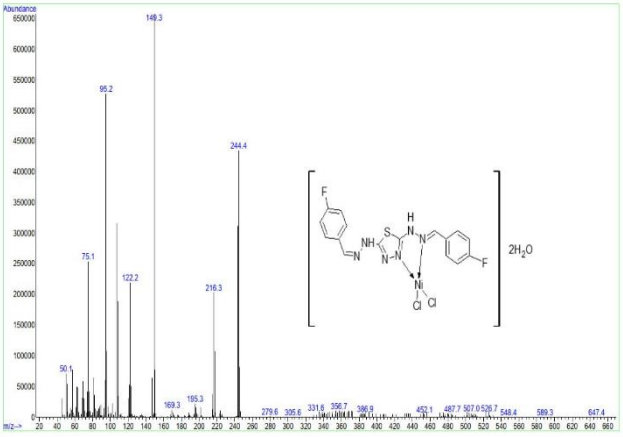

Figure 10: Mass spectrum of NiL_2

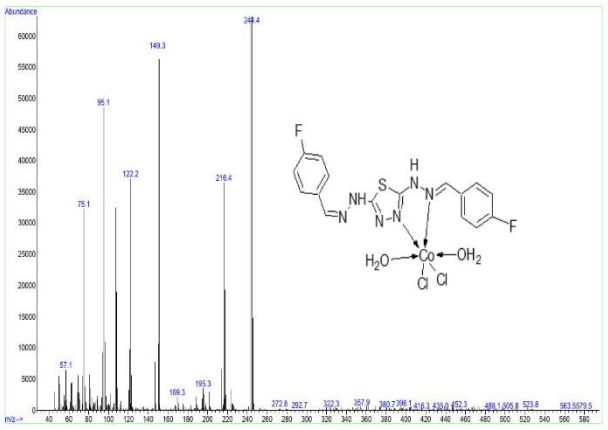

Figure 9: Mass spectrum of CuL_2

4- UV–Visible Spectroscopy (UV–Vis)

Electron absorption spectra of these bonds, synthesized in dimethylformamide (DMF) at a concentration of 1×10^{-4} M, were obtained in the 200–800 nm range. The presence of several conjugated chromophore units, including a phenyl ring, an azomethine (C=N) bond, and a thiadiazole ring, resulted in characteristic π→π* and n→π* electron transitions in these bonds. In general, π→π* transitions were observed at shorter wavelengths with relatively high absorption intensities, while n→π* transitions were observed at longer wavelengths with relatively low absorption intensities. Particular attention was paid to the extended π conjugation and the presence of heteroatoms, especially the presence of non-bonding electron pairs. The determination of the absorption bands was based on the observed λmax values[34] . In particular, the presence of non-bonding electron pairs in the electronic distribution can lead to overlap or convergence of absorption bands, especially those corresponding to the azomethine group and the thiadiazole ring.

UV–Visible Spectra of Ligand L_2 and Its Metal Complexes

As shown in **Table 12** and **Figures 11–14**, the L2 ligand exhibited four absorption bands at 280, 285, 293, and 389 nm, with molar absorbance values (ε) of 3970, 6270, 6450, and 6540 L/mol/cm², respectively. The band centered at 389 nm was identified as an n→π* transition, while the bands at 293, 285, and 280 nm were attributed to π→π* transitions of the azomethine group, the thiadiazole ring, and the phenyl ring, respectively [35]. The relatively large molar absorbance values are consistent with the presence of allowed electron transitions associated with the extended π-conjugated system of the ligand. The π→π* transitions showed only slight wavelength changes, indicating changes in the electronic environment after complex formation when bonded to cobalt(II), nickel(II), and copper(II) ions, respectively. However, the n→π* band showed a shift towards shorter wavelengths, from 389 nm for the free linker to 376, 388, and 375 nm for CoL2, NiL2, and CuL2, respectively, suggesting the involvement of a nitrogen donor atom in the bonding to the metal center [36]. Furthermore, a new band appeared at approximately 348, 335, and 335 nm for CoL2, NiL2, and CuL2, respectively, which was attributed to a charge transfer from the linker to the metal (LMCT) [37]. The CoL2 complex recorded two beams at 520 and 897 nm, and the NiL2 complex showed a transition at 758 nm, while the CuL2 complex recorded one beam at 759 nm [38]. The relatively low intensity of these beams is a characteristic feature of d-d transitions that are forbidden according to Laporte's rule, and is consistent with the proposed symmetry geometry of the synthesized compounds [39].

Table 9: UV–Visible Spectra of Ligand L_2 and Its Metal Complexes

Comp.	λmax (nm)	Abs.	ε L.mol^{-1}.cm^{-1}	Transitions and assignment
L_2	389	0.654	6540	n→π*
	293	0.645	6450	π→π* (C=N) Azo
	285	0.627	6270	π→π*(C=N) 1,3,4-Thiadiazole ring
	280	0.397	3970	π→π* (C=C) Phenyl ring
coL_2	897	0.030	300	(d-d Transition)
	520	0.019	190	(d-d Transition)
	376	0.202	2020	n→π*
	348	0.482	4820	Charge Transfer(CT)
	296	0.287	2870	π→π* (C=N) Azo
	287	0.305	3050	π→π*(C=N) 1,3,4-Thiadiazole ring
	282	0.311	3110	π→π* (C=C) Phenyl ring
NiL_2	758	0.060	600	(d-d Transition)
	388	0.353	3530	n→π*
	335	0.724	7240	Charge Transfer(CT)
	326	0.749	7490	π→π* (C=N) Azo
	296	0.717	7170	π→π*(C=N) 1,3,4-Thiadiazole ring
	287	0.716	7160	π→π* (C=C) Phenyl ring
cuL_2	759	0.029	290	(d-d Transition)
	375	0.165	1650	n→π*
	335	0.522	5220	Charge Transfer(CT)
	287	0.453	4530	π→π* (C=N) Azo
	285	0.455	4550	π→π*(C=N) 1,3,4-Thiadiazole ring
	280	0.466	4660	π→π* (C=C) Phenyl ring

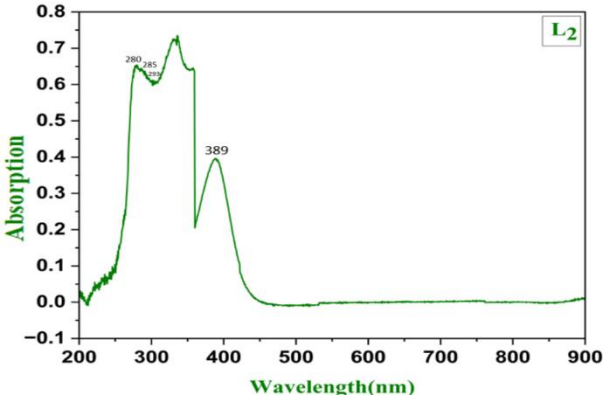

Figure 12: UV–Visible Spectrum of L_2

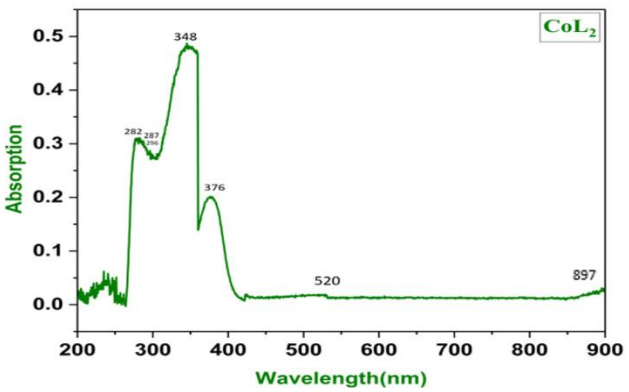

Figure 11: UV–Visible spectrum of CoL_2

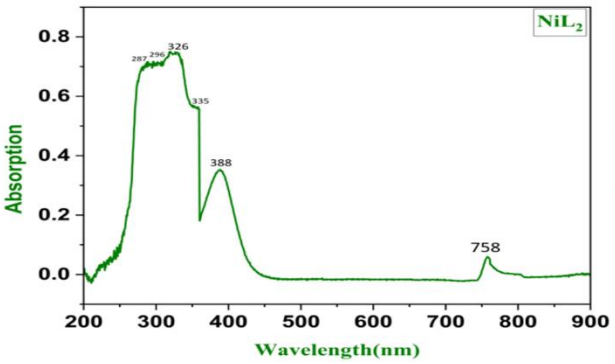

Figure 14: UV–Visible spectrum of NiL_2

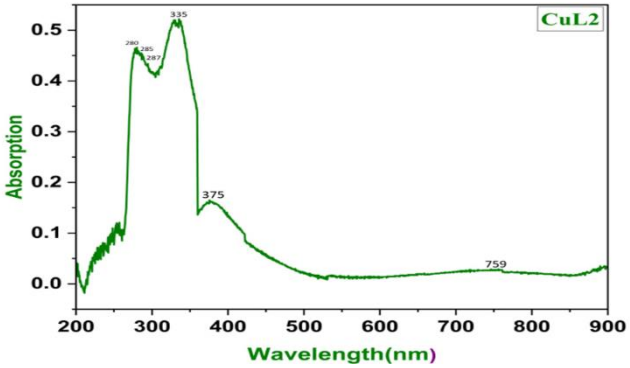

Figure 13: UV–Visible spectrum of CuL_2

5-Molar Conductivity

As shown in **Table 13**, molar conductivity data proved useful in determining the ionic nature of coordination compounds and whether there were antiparallel ions in the outer shell. The measured molar conductivity values showed that all the synthesized metal complexes were non-electrolytes in solution, implying the absence of ions in the outer shell [40].

These results were further confirmed by the silver nitrate ($AgNO_3$) assay, where no white precipitate or cloudiness was observed after the addition of the reagent to the complex solutions [41].

Table 10: Molar electrical conductivity of the prepared complexes.

NO.	Complexes	Λm (s.cm^2.mole^{-1})	Electrolyte type
1	**CoL_2**	**8.6**	**Non electrolyte**
2	**NiL_2**	**9.4**	**Non electrolyte**
3	**CuL_2**	**10.2**	**Non electrolyte**

6- Cyclic Voltammetry (CV)

In **Figures 15–17** and **Table 14**, the electrochemical properties of these L2 bonds, and their compounds with cobalt(II), nickel(II), and copper(II), as well as with the salts of the primary metals ($CoCl_2 \cdot 6H_2O$, $NiCl_2 \cdot 6H_2O$, and $CuCl_2 \cdot 6H_2O$), were explored using cyclic voltammetry (CV) in a 0.1 M solution of tetrabutylammonium perchlorate (TBAP) in dimethylformamide (DMF) under an argon atmosphere at room temperature. The electrochemical measurements were performed using a conventional three-electrode single-chamber cell consisting of a 3 mm diameter, freshly polished glassy carbon disk as the working electrode, a platinum wire as the counter electrode, and a silver pseudo-reference electrode. The comparator electrode was calibrated using the redox pair Fc^+/Fc in dimethylformamide (DMF), yielding a formal potential of +0.07 V under the experimental conditions, with solution resistance (iR) compensation automatically applied throughout the measurements [42]. Prior to each experiment, the working electrode was polished with 0.05 μm alumina paste, thoroughly rinsed with distilled water, and finally washed with DMF. All voltamgrams were recorded at a scan rate of 100 mV/s, and all reported potentials were calibrated relative to a silver pseudo-comparator electrode [43].

Table 11: Cyclic Voltammetry of Ligand L_1 and Its Metal Complexes

compound	Concentration (mM)	Voltage Scan rate (V/S)	Ep_c (V)	ip_c (µA)	Ep_c	ip_a (µA)	$E_{1/2}$ (V)	ΔEp (V)	ip_a/ip_c (µA)
L_2	2	0.1	-1.383 <-1.988 -2.288 --- --- --- --- --- ---	135.065 107.147 -36.835 --- --- --- --- --- ---	≈-1.311 --- --- ≈-2.144 ≈-1.823 -0.589 -0.136 1.13 ≈1.727	155.182 --- --- 116.264 140.517 160.326 173.732 35.294 49.28	-1.347 --- --- --- --- --- --- --- ---	0.072 --- --- --- --- --- --- --- ---	1.148 --- --- --- --- --- --- --- ---
CoL_2	2	0.1	-1.211 -1.381 -2.299 --- --- --- --- --- --- ---	-26.124 -90.515 -156.963 --- --- --- --- --- --- ---	--- ≈-1.301 --- ≈-2.157 ≈-1.834 -0.599 -0.146 1.103 ≈1.708 ≈1.136	--- -16.047 --- -78.407 -133.989 -5.911 10.736 84.298 33.783 11.065	--- --- --- --- --- --- --- --- --- ---	--- --- --- --- --- --- --- --- --- ---	--- --- --- --- --- --- --- --- --- ---
NiL_2	2	0.1	-1.396 ≈-1.903 -2.359 --- ---	-90.336 -38.192 -20.533 --- --- --- ---	≈-1.324 --- --- >-2.147 ≈-1.801 -0.515 1.108	-14.313 --- --- -31.514 -24.114 13.639 37.931	-1.36 --- --- --- --- --- --- ---	0.072 --- --- --- --- --- --- ---	0.158 --- --- --- --- --- --- ---

			--- --- ---	---	≈1.655	38.537	---	---	---
CoL_2	2	0.1	-1.445 ≈-1.968 <-2.343 --- --- --- ---	-66.691 -23.57 -62.468 --- --- --- ---	-1.323 --- --- ≈-2.243 ≈-1.854 -0.399 ≈1.023	5.918 --- --- -25.126 -16.625 14.646 11.711	-1.384 --- --- --- --- --- ---	0.122 --- --- --- --- --- ---	-0.088 --- --- --- --- --- ---
$CoCl_2.6H_2O$	3	0.1	-1.06 -1.205 <-1.213 -1.718 --- ≈1.032	-11.907 -4.01 -3.734 -8.963 --- -6.019	--- -1.221 --- --- 1.51 ---	--- 51.16 --- --- 116.943 ---	--- -1.213 --- --- --- ---	--- -0.016 --- --- --- ---	--- 12.758 --- --- --- ---
$NiCl_2.6H_2O$	3	0.1	-0.913 --- ---	-111.805 --- ---	--- ≈-2.173 1.627	--- -28.843 99.833	--- --- ---	--- --- ---	--- --- ---
$CuCl_2.6H_2O$	3	0.1	-0.301 -0.510 <-1.55 ≈-2.15 --- ---	-6.204 -2.923 3.382 -21.814 --- ---	--- --- --- --- -0.39 ≈1.15	--- --- --- --- 61.601 17.956	--- --- --- --- --- ---	--- --- --- --- --- ---	--- --- --- --- --- ---

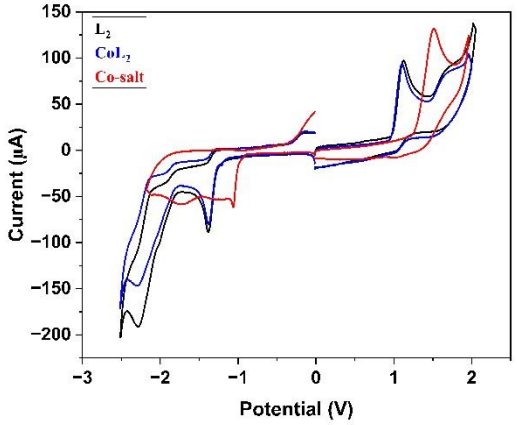

Figure 16: Cyclic Voltammetry of L_2, CoL_2, $CoCl_2.6H_2O$

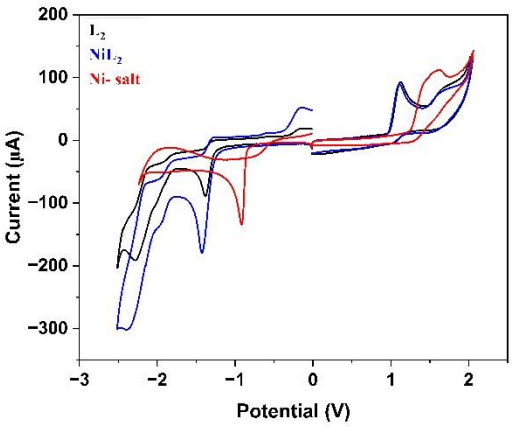

Figure 15: Cyclic Voltammetry of L_2, NiL_2, $NiCl_2.6H_2O$

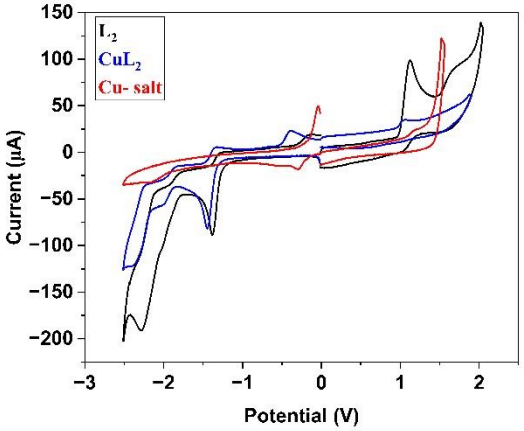

Figure 17: Cyclic Voltammetry of L_1, CuL_1, $CuCl_2.6H_2O$

e recorded and depicted in **Figures 15 to 17,** respectively. The first cathodic peak potential (E_{pc}^1) of the L_2 ligand (-1.383 V) is cathodically shifted (hardly happened) to -1.396 V and -1.445 V for NiL_2 and CuL_2, respectively, due to a decrease in electron density of the ligand L_2 upon complexation. The easier first reduction of CoL_2 compared with the free L_2 ligand (unlike other complexes: NiL_2 and CuL_2) is assigned to back-bonding. While the second reduction (E_{pc}^2) of L_2 complexes happened hardly compared with that (-2.288 V) of the free L_2 ligand [44]. This is attributed to the stability of complexed $L_2^{-\cdot}$ (formed after the first reduction) compared with the free $L_2^{-\cdot}$ Stability increases in the order: $CoL_2 < CuL_2 < NiL_2$. Therefore, the E_{pc}^2 were -2.299 V, -2.343 V and -2.359 V for CoL_2, CuL_2 and NiL_2, respectively. Interestingly, an anodic process appeared and increased in difficulty in the order: free L_2 (-0.136 V), CoL_2 (-0.146 V), CuL_2 (-0.399 V) and NiL_2 (-0.515 V). The first oxidation (E_{pc}^1) of the complexed L_2 ligand is cathodically (easier oxidation) shifted compared to that of the free ligand (1.13 V). This trend could be assigned to back-bonding. Therefore, the E_{pc}^1 is noted at ≈1.023 V, 1.103 V and 1.108 V for CuL_2, CoL_2, and NiL_2, respectively. The second oxidation potential of the complexed L_2 ligand is also cathodically shifted compared to that of the free L_2 ligand.

The biocapacity of the metal salt was recorded and presented in Figures 15–16. The peak redox potentials are shown in Table 14. No redox behavior was observed for these metals in their complexes. The first, easier reduction (Epc1) of the complex corresponds to a higher electron density requirement, i.e., a lower electron density for the complex ligand. Therefore, the electron density increases in the following sequence: CoL2 < NiL2 < CuL2. CoL2 has the highest electron density, while CuL2 has the lowest among the complexes. A high Epc2 indicates a high Ln- complex. Stability is established after the first reduction. Epc2 values increase in the following order: CoL2 < CuL1 < CuL2 < NiL2. Therefore, Ln- increases in stability after the last sequence. The present electrical study: differences in redox behaviors among ligands and those among ligands and their complexes, emergence and absence

of some redox processes show and support undoubtedly the electron densities, stabilities, complex formation, electron delocalization, and back bonding [45].

7- Computational Analysis of the Electron Density Distribution

The Gaussian package was used for computational calculations, while GaussView 6.0 was used to construct and image the molecular structures. Electron density calculations were performed on the prepared bond to study the electron density distribution and identify the most probable coordination sites. The proposed metal complexes were constructed and imaged, but no quantitative chemical calculations were performed on them [46]. As shown in **Figures 18–22**, theoretical and spectroscopic studies revealed that the copper(II) and nickel(II) complexes favor a tetrahedral geometry, while the cobalt(II) complexes exhibit an octahedral geometry [47].

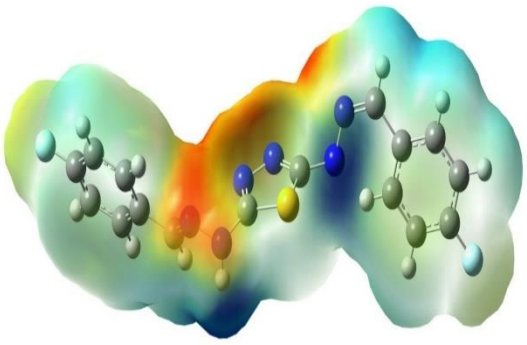

Figure 19: L_2 of EMP

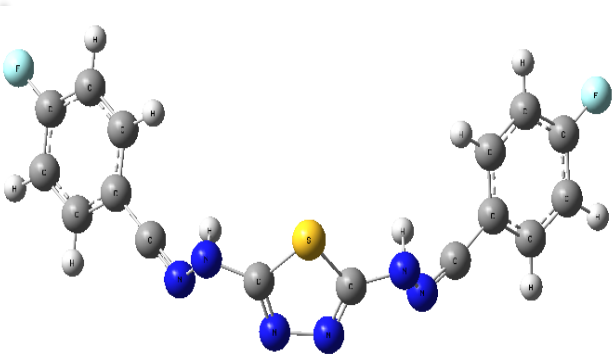

Figure 18: Molecular Structure of L_2

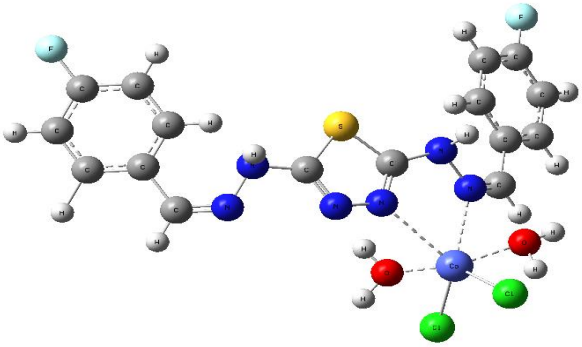

Figure 21: Molecular Structure of CoL_2

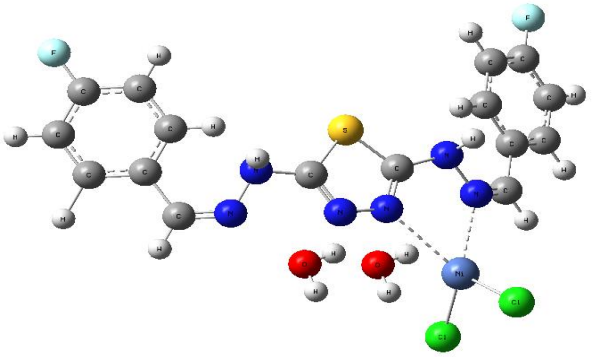

Figure 20: Molecular Structure of NiL_2

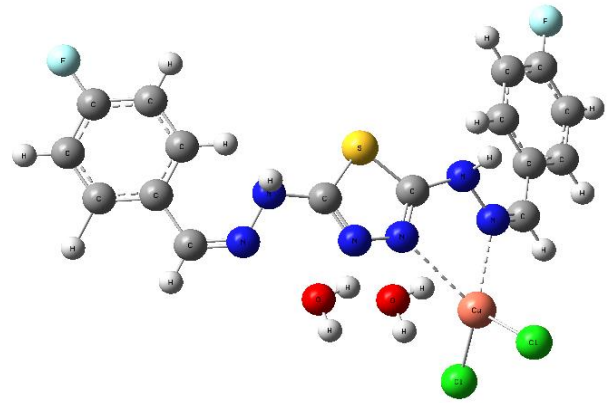

Figure 22: Molecular Structure of CuL_2

8-Anticancer Activity

The synthesized ligand was tested for its in vitro anticancer activity against MCF-7 cells. The HBL-100 cell line, a non-cancerous human mammary epithelial cell line, was used as a normal cell model to evaluate the toxicity and selectivity of the synthesized compound. Both cell lines were used to compare the synthesized compound's effect on cancer cell growth with its toxicity to normal cells [48].

The effect of L2 ligand on the corresponding proliferative inhibition results is shown in **Figure 23**. L2 ligand was tested on the human MCF-7 breast cancer cell line to determine its anticancer activity. The results indicated that the ligand did not inhibit growth by 50% at any of the tested concentrations (15, 30, and 45 μg/ml). That is, the IC_{50} value could not be determined, and the L2 ligand was not active within the studied concentration range [49]. These results suggest the need for further testing at higher concentrations to determine the potential for increased growth inhibition. Comparing L2 with other cancer cell lines may help to explain its biological activity, as cellular responses may differ between tumor types [50].

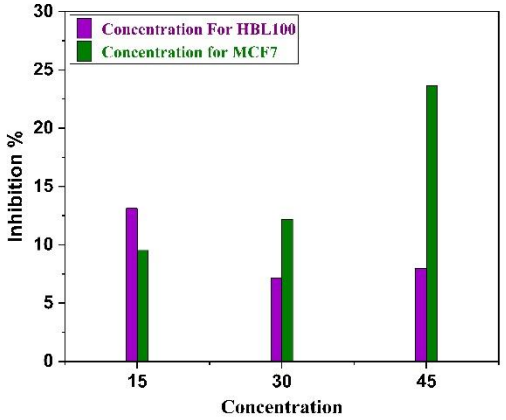

Figure 23: Anticancer activity of L_1 against MCF-7 breast cancer cells and HBL-100 normal cells

Conclusions

Analytical and spectroscopic results confirmed the proposed molecular structures of the 1,3,4-thiadiazole-based ligands and their metal complexes with cobalt(II), nickel(II), and copper(II) ions. These results were obtained using a comprehensive suite of techniques, including Fourier transform infrared (FT-IR) spectroscopy, ultraviolet-visible (UV-Vis) spectroscopy, proton/carbon-13 nuclear magnetic resonance ($^{1}H/^{13}C$ NMR), mass spectrometry, and molar conductivity measurements. The electrical conductivity measurements revealed that the prepared complexes exhibit a non-electrolyte nature, indicating the absence of corresponding ions isolated from the coordination domain. This provides further support for the proposed complex structures. Molecular modeling using Gaussian software and the GaussView 6.0 interface enabled the determination of the weighted coordination positions of the ligand and metal ions. The results indicated that the nickel(II) and copper(II) complexes exhibited a tetrahedral geometry, while the cobalt(II) complex likely possessed an octahedral geometry. Cyclic voltammetry (CV) analysis revealed a clear difference in the electrochemical behavior of the ligands compared to their metal complexes. The binding of the metal ion to the ligand led to a significant change in the characteristics of the reduction and oxidation processes, as well as in the nature of the electronic configuration. This confirms that the type of metal ion and its compatibility with the ligand play a crucial role in determining the electronic and electrochemical properties of the studied systems. From a biological perspective, the activity of the prepared ligands was evaluated against the human breast cancer cell lines MCF-7 and HBL100. The results showed that the inhibitory effect on cell growth remained limited within the range of concentrations used in the study, as a 50% inhibition of cell viability was not achieved. Therefore, it was not possible to determine IC_{50} values under the experimental conditions.

Acknowledgements

Professors of the Chemistry Department, College of Science, University of Thi Qar, Iraq

Declaration of generative AI in scientific writing

Some artificial intelligence tools were used in text rewriting and grammatical language improvement.

References

[1] A. M. Daoud, "Synthesis, characterization and evaluation biological activity of new Schiff base compounds and their complexes with some transition elements," *University of Thi-Qar Journal of Science,* vol. 6, no. 2, pp. 81-90, 2017.

[2] A. H. Katea, "Synthesis, Characterization, Antimicrobial New 2, 2'-[(1E, 2E)-ethane-1, 2-diylidenedi (2E) hydrazin-1-yl-2-ylidene] bis (5-methyl-1, 3, 4-oxadiazole) and their transition metal complexes," *University of Thi-Qar Journal of Science,* vol. 6, no. 2, pp. 1-18, 2017.

[3] N. A. A. Alkafiji, "Preparation, Characterization and Biological Study of New Derivatives of 1, 3, 4-Thiadiazoleand Its Complexes with Some Transitional Element Ions," *University of Thi-Qar Journal of Science,* vol. 6, no. 3, pp. 90-100, 2017.

[4] A. K. Jain, S. Sharma, A. Vaidya, V. Ravichandran, and R. K. Agrawal, "1, 3, 4-Thiadiazole and its derivatives: A review on recent progress in biological activities," *Chemical biology & drug design,* vol. 81, no. 5, pp. 557-576, 2013.

[5] Y. Hu, C.-Y. Li, X.-M. Wang, Y.-H. Yang, and H.-L. Zhu, "1, 3, 4-Thiadiazole: synthesis, reactions, and applications in medicinal, agricultural, and materials chemistry," *Chemical reviews,* vol. 114, no. 10, pp. 5572-5610, 2014.

[6] S. Indelicato, D. Bongiorno, M. Mauro, and S. Cascioferro, "Recent developments of 1, 3, 4-thiadiazole compounds as anticancer agents," *Pharmaceuticals,* vol. 18, no. 4, p. 580, 2025.

[7] S. Daravath, M. P. Kumar, A. Rambabu, N. Vamsikrishna, and N. Ganji, "Design, synthesis, spectral characterization, DNA interaction and biological activity studies of copper (II), cobalt (II) and nickel (II) complexes of 6-amino benzothiazole derivatives," *Journal of Molecular Structure,* vol. 1144, pp. 147-158, 2017.

[8] M. Kuate *et al.*, "Synthesis, Characterization, Cyclic Voltammetry, and Biological Studies of Co (II), Ni (II), and Cu (II) Complexes of a Tridentate Schiff Base, 1-((E)-(2-Mercaptophenylimino) Methyl) Naphthalen-2-ol (H2L1)," *Journal of Chemistry,* vol. 2020, no. 1, p. 5238501, 2020.

[9] G. Venkatesh *et al.*, "Synthesis and spectroscopic characterization of Schiff base metal complexes, biological activity, and molecular docking studies," *ACS omega,* vol. 9, no. 7, p. 8123, 2024.

[10] M. Pervaiz *et al.*, "Thiosemicarbazides, 1, 3, 4 thiadiazole Schiff base derivatives of transition metal complexes as antimicrobial agents," *Inorganic Chemistry Communications,* vol. 160, p. 111856, 2024.

[11] A. Rani, J. Sharma, S. K. Ramasamy, R. V. Saini, R. Khanna, and E. Sharma, "Synthesis, Antimicrobial, Anticancer, and Molecular Docking Studies of Transition Metal Complexes of Thiadiazole-Based Schiff Base," *ChemistrySelect,* vol. 10, no. 32, p. e02737, 2025.

[12] A. M. Abu-Dief *et al.*, "Strategic design and bioactive potential of some novel thiazole-based bi-dentate metal complexes: integrated spectroscopic, DFT, and molecular docking investigations," *Journal of the Indian Chemical Society,* vol. 102, no. 10, p. 102036, 2025.

[13] L. G. Lavrenova *et al.*, "Synthesis, structure, and magnetic and biological properties of copper (II) complexes with 1, 3, 4-thiadiazole derivatives," *International Journal of Molecular Sciences*, vol. 24, no. 16, p. 13024, 2023.

[14] V. Manakkadan *et al.*, "Copper-mediated cyclization of thiosemicarbazones leading to 1, 3, 4-thiadiazoles: Structural elucidation, DFT calculations, in vitro biological evaluation and in silico evaluation studies," *Spectrochimica Acta Part A: Molecular and Biomolecular Spectroscopy*, vol. 313, p. 124117, 2024.

[15] W. Zhou, J. Ge, W. Zhang, M. Li, Q. Zheng, and Y. Zhang, "Engineering high mechanical strength and synergistically antibacterial PDMS coatings via a “rivet-like” metal coordination strategy," *Journal of Macromolecular Science, Part A*, vol. 63, no. 6, pp. 493-505, 2026.

[16] L. A. Naser, A. Al-Ghazzi, and R. MAHMOOD, "Synthesis, Spectroscopic and Nano-Structural Characterization, Molecular Docking, and Corrosion Inhibition Studies of Novel Nano-Schiff Base Ligands Derived from 2-Aminobenzothiazole and Substituted Salicylaldehyde," *Journal of Nanostructures*, vol. 16, no. 3, pp. 3706-3717, 2026.

[17] G. S. Ruziboyeva *et al.*, "An oxo-bridged trinuclear nickel (II) cluster supported by 1, 3, 4-thiadiazole-2, 5-diamine: Crystal structure, multitechnique characterization and antimicrobial activity," *Journal of Cluster Science*, vol. 37, no. 2, p. 45, 2026.

[18] H. S. Sayiner *et al.*, "Synthesis and characterization of new 1, 3, 4-thiadiazole derivatives: study of their antibacterial activity and CT-DNA binding," *RSC advances*, vol. 12, no. 46, pp. 29627-29639, 2022.

[19] B. TORAMBETOV and S. KADİROVA, "RECENT ADVANCES IN 1, 3, 4-THIADIAZOLE-BASED METAL COMPLEXES: COORDINATION CHEMISTRY, CRYSTAL STRUCTURES, AND BIOLOGICAL ACTIVITIES," *An overview of Coordination Chemistry with Metals, Ligands, Complexes and Applications: In Honor of Hacali Necefoğlu’s 70th Birthday*, p. 101, 2025.

[20] M. Soleiman-Beigi, M. Alikarami, H. Kohzadi, and Z. Akbari, "Dipotassium 1, 3, 4-thiadiazole-2, 5-bis (thiolate) as a new S-donor for direct synthesis of symmetrical disulfides," *Scientific Reports*, vol. 12, no. 1, p. 16149, 2022.

[21] N. Rezki, A. M. Al-Yahyawi, S. K. Bardaweel, F. F. Al-Blewi, and M. R. Aouad, "Synthesis of novel 2, 5-disubstituted-1, 3, 4-thiadiazoles clubbed 1, 2, 4-triazole, 1, 3, 4-thiadiazole, 1, 3, 4-oxadiazole and/or Schiff base as potential antimicrobial and antiproliferative agents," *Molecules*, vol. 20, no. 9, pp. 16048-16067, 2015.

[22] D. Kumar, N. Aggarwal, V. Kumar, H. Chopra, R. K. Marwaha, and R. Sharma, "Emerging synthetic strategies and pharmacological insights of 1, 3, 4-thiadiazole derivatives: a comprehensive review," *Future Medicinal Chemistry*, vol. 16, no. 6, pp. 563-581, 2024.

[23] D. S. Azeez and M. A. Abbas, "Synthesis, Characterizations and Computational Studies of Metal Ion Complexes Containing Siderphore Analogs and Study of Biosynthesis Siderphores by Pseudomonas Aeruginosa," 2025.

[24] C. A. Herbert and E. R. Jarvo, "Nickel-catalyzed stereoselective coupling reactions of benzylic and alkyl alcohol derivatives," *Accounts of Chemical Research*, vol. 56, no. 22, p. 3313, 2023.

[25] S. S. Badade, D. N. Pansare, R. N. Shelke, P. Kashid, and S. R. Bembalkar, "Synthesis and Antimicrobial Screening of Metal-ligand Complexes Derivative from (2-chloroquinolin-3-yl) methylene) hydrazine) and their Biological Studies," *Oriental Journal of Chemistry*, vol. 41, no. 3, 2025.

[26] L. Yue, M. G. Debije, and A. P. Schenning, "Stimuli-responsive afterglow from luminescent liquid crystal elastomers," *Advanced Materials*, vol. 38, no. 7, p. e16922, 2026.

[27] S. Abbas *et al.*, "Design, synthesis, biological assessment, and in silico analysis of bisthiazolidine amide derivatives as potential anti-bacterial and anti-prostate cancer agents," *Green Chemistry Letters and Reviews*, vol. 18, no. 1, p. 2541058, 2025.

[28] A. S. Temma, O. N. Ali, R. H. Al-Asadi, and M. K. Mohammed, "Evaluation of Schiff Bases Against Two Cancer Cell Lines: A Combined Experimental and Theoretical Approach," *Tropical Journal of Natural Product Research*, vol. 9, no. 3, p. 967, 2025.

[29] W.-D. Lin *et al.*, "Structural and functional characterization of Pin1BP1: A novel Pin1-interacting protein regulating apoptosis," *International Journal of Biological Macromolecules*, vol. 319, p. 145587, 2025.

[30] R. Dulare, "Biological Activities of 1, 3, 4-Thiadiazole Derivatives," 2025.

[31] A. M. El-Saghier *et al.*, "Thiadiazole/thiadiazine derivatives as insecticidal agent: design, synthesis, and biological assessment of 1, 3, 4-(thiadiazine/thiadiazole)-benzenesulfonamide derivatives as IGRs analogues against Spodoptera littoralis," *Journal of Agricultural and Food Chemistry*, vol. 72, no. 20, pp. 11369-11380, 2024.

[32] M. Sallam, A. M. Metwaly, and E. A. E.-W. Ragab, "UPLC-Triple TOF-MS/MS Phytochemical Profiling and In Vitro Evaluation of Saraca cauliflora Bak. Methanolic Leaf Extract," *Egyptian Journal of Chemistry*, 2025.

[33] A. G. Abdulrazzaq, S. S. Abood, and A. A. S. Al-Hamdani, "Synthesis, characterization, thermal analysis and antioxidant determination for some metal ions complexes with new ligand," *Bulletin of the Chemical Society of Ethiopia*, vol. 39, no. 11, pp. 2129-2144, 2025.

[34] F. Ejiah, M. Rofiu, A. Akitoye, and T. Fasina, "Synthesis, characterization and electrochemical studies of Schiff bases containing 4-aminobenzoic acid MOEITY," *Journal of Chemical Society of Nigeria*, vol. 49, no. 2, 2024.

[35] R. Venkatesh *et al.*, "Exploring the chemical and biological landscape of a Nickel (II) schiff base complex via azomethine linkage," *Scientific Reports*, vol. 16, no. 1, p. 2256, 2025.

[36] B. Es-Sounni *et al.*, "Synthesis, characterization, antioxidant and antibacterial activities of six metal complexes based tetradentate salen type bis-Schiff base," *Biointerface Res. Appl. Chem*, vol. 13, no. 4, p. 333, 2023.

[37] Q. T. Nguyen, P. N. Pham Thi, and V. T. Nguyen, "Synthesis, characterization, and in vitro cytotoxicity of unsymmetrical tetradentate Schiff base Cu (II) and Fe (III) complexes," *Bioinorganic chemistry and applications*, vol. 2021, no. 1, p. 6696344, 2021.

[38] V. Borghesani, M. L. Zastrow, A. E. Tolbert, A. Deb, J. E. Penner-Hahn, and V. L. Pecoraro, "Co (II) substitution enhances the esterase activity of a de novo designed Zn (II) carbonic anhydrase," *Chemistry–A European Journal*, vol. 30, no. 24, p. e202304367, 2024.

[39] H. W. M. Arifin *et al.*, "A selective fluorescent chemosensor based on chromone hydrazone ligand for Zinc ions," *Central Asia & the Caucasus (14046091)*, vol. 23, no. 1, p. 2011, 2022.

[40] B. R. C. Kumar, K. S. Babu, and P. Shabana, "SYNTHESIS, CHARACTERIZATION, AND BIOLOGICAL EVALUATION OF NOVEL HETEROCYCLIC PYRIDINE BASED THIOPHENE DERIVATIVE OF TRANSITION METAL COMPLEXES," *European Journal of Biomedical*, vol. 9, no. 1, pp. 278-288, 2022.

[41] R. Jalilov and N. Khudoyberdieva, "Influence of geometric parameters of granular particles on fluidization quality," in *Optical and Computational Technologies for Measurements and Industrial Applications (OptiComp 2025)*, 2025, vol. 13803: SPIE, pp. 621-626.

[42] A. H. Al-Taher, H. K. Mejbel, L. F. Al-Badry, and W. S. Abdul-Hassan, "Influence of end groups (4F, 4Br, 4CF3, and 4CBr3) of non-fullerene acceptor molecules on the performance of organic solar cells," *Journal of Nanoparticle Research*, vol. 27, no. 4, p. 96, 2025.

[43] A. A. Alibrahimi and W. S. Abdul-Hassan, "Design and Synthesis of Novel Molecular Switches Functionalized with a Viologen Unit Based on Copper (II) Bis (ethyl 4-chloroacetoacetate) Complex," *EURASIAN JOURNAL OF CHEMISTRY,* vol. 31, no. 2 (122), pp. 16-40, 2026.

[44] M. A. Muhamed and H. W. S. Abdul, "Iron (II), cobalt (II), and nickel (II) complexes of bis-(3-chloroacetylacetonate) ethylenediimine and bis-(acetylacetonate) ethylenediimine and their viologen molecular switches," 2023.

[45] A. A. Alibrahimi and W. S. Abdul-Hassan, "Molecular Switches Incorporating the Adducts Among Viologen unints and both Copper Bis (ethylacetoacetate) and Copper Bis (ethyl 4-chloroacetoacetate)," *Vascular and Endovascular Review,* vol. 8, no. 6s, pp. 151-182, 2025.

[46] S. J. Kabilan, O. Sivakumar, S. Kunjiappan, P. Pavadai, and K. Sundar, "Molecular modelling approaches for the identification of potent sodium-glucose cotransporter 2 inhibitors from Boerhavia diffusa for the potential treatment of chronic kidney disease," *Journal of Research in Pharmacy,* vol. 29, no. 5, pp. 1851-1877, 2025.

[47] C. Santhosh, K. R. Singh, K. Sheela, T. R. Swaroop, and M. P. Sadashiva, "Regioselective synthesis of 2, 5-disubstituted-1, 3, 4-thiadiazoles and 1, 3, 4-oxadiazoles via alkyl 2-(methylthio)-2-thioxoacetates and alkyl 2-amino-2-thioxoacetates," *The Journal of Organic Chemistry,* vol. 88, no. 16, pp. 11486-11496, 2023.

[48] R. K. Mittal, R. Mishra, V. Sharma, and I. Mishra, "1, 3, 4-thiadiazole: A versatile scaffold for drug discovery," *Letters in Organic Chemistry,* vol. 21, no. 5, pp. 400-413, 2024.

[49] S. Janowska *et al.*, "Synthesis and anticancer activity of 1, 3, 4-thiadiazoles with 3-methoxyphenyl substituent," *Molecules,* vol. 27, no. 20, p. 6977, 2022.

[50] S. Janowska *et al.*, "New 1, 3, 4-thiadiazole derivatives with anticancer activity," *Molecules,* vol. 27, no. 6, p. 1814, 2022.